Journal of Magnetic Resonance **144,** 372–377 (2000)
doi:10.1006/jmre.2000.2078, available online at http://www.idealibrary.com on IDEAL®

Chemical Shift Imaging with Continuously Flowing Hyperpolarized Xenon for the Characterization of Materials[1]

Igor L. Moudrakovski,* Stephen Lang,*,† Christopher I. Ratcliffe,* Benoit Simard,* Giles Santyr,† and John A. Ripmeester*,[2]

*Steacie Institute for Molecular Sciences, National Research Council of Canada, Ottawa, Ontario, Canada K1A 0R6, and †Department of Physics, Carleton University, Ottawa, Ontario, Canada K1S 5B6

Received December 31, 1999; revised March 2, 2000

In this contribution we report new approaches to the MRI of materials using continuously produced laser-polarized ^{129}Xe gas. This leads to vastly improved sensitivity and makes new kinds of information available. The hyperpolarized xenon is produced in a continuous flow system that conveniently delivers the xenon at low partial pressure to probes for NMR and MRI experiments. We illustrate applications to the study of micropore and other kinds of void space and show for the first time that with flowing hyperpolarized xenon it is possible to obtain chemical-shift-resolved images in a relatively short time. © 2000 Academic Press

Key Words: **laser-polarized xenon; continuous flow; porous materials; chemical shift imaging.**

INTRODUCTION

^{129}Xe NMR of adsorbed xenon has proven to be a valuable tool for the study of microporous materials (*1–3*). The high sensitivity of the chemical shift to the local environment makes ^{129}Xe NMR a very useful method for testing different aspects of the structure and chemistry of porous solids (*3*). A firm theoretical basis for the interpretation of the shift has been laid by the work of Jameson *et al.* (*4*).

Limited sensitivity has always been a problem in the application of ^{129}Xe to study materials. An increase in sensitivity of several orders of magnitude can be achieved by using optical pumping techniques for the production of hyperpolarized (HP) xenon (*5*). This has been used to good advantage in the development of HP xenon imaging for clinical applications, especially lung imaging (*6*). For materials applications, recent advances include examples of HP Xe delivery into MAS probes (*7*) and of a recirculating continuous flow system that offers prospects for the recording of Xe spectra of materials in a closed system (*8–10*).

There have been several attempts to image materials with hyperpolarized xenon. Most of these deal with fairly simple model systems, such as various arrangements of void spaces assembled from materials with suitable relaxation properties. Only in two cases have materials with potentially useful properties been imaged: aerogel in one instance (*11*) and open-cell foams in another (*10*). A serious problem that limits applications of HP Xe imaging of materials to a narrow set of carefully selected systems is the nonrenewable character of the nonequilibrium polarization. Many materials of interest possess paramagnetic centers that have a profound depolarizing effect. Once the hyperpolarized gas is brought into contact with the material, all polarization may be lost in a very short time (often in a matter of a few seconds) through the mechanisms of spin–lattice relaxation. Mainly this is a limitation of experiments that use hyperpolarized gas produced in a batch mode. With the use of a continuous flow apparatus this drawback can be made less important, as was recently demonstrated by employing a closed recirculating system (*8–10*).

A more serious barrier to imaging with hyperpolarized gases is the limited number of contrast variables. To date, for most images produced with hyperpolarized gases the contrast arises mainly from gas density. The development of better contrast mechanisms will undoubtedly increase the usefulness of the technique and expand the scope for applications. Recent progress in this direction include the use of T_2^* diffusion contrast for HP gas in lungs (*12*) and chemical shift resolved imaging of HP Xe in a rat's brain (*13*).

Because of the high sensitivity of the ^{129}Xe chemical shift to the local environment in voids, chemical shift imaging (CSI) of ^{129}Xe promises to be an excellent tool for differentiating distinct regions. This has been demonstrated recently with thermally polarized xenon in aerogels (*14*). However, the very low sensitivity required extremely long data acquisition times (on the order of some tens of hours) and necessitated the use of high Xe pressures. Such requirements are likely to limit this approach for general use.

In this Communication we show that with the use of optically polarized xenon produced in a continuous flow, the CS imaging of various adsorbents can be performed with drastically reduced acquisition times. We report on the use of a

[1] Issued as NRCC No. 43834.

[2] To whom correspondence should be addressed at 100 Sussex Drive, Ottawa, Ontario, K1A 0R6, Canada. Fax: (613) 998 7833. E-mail: jar@ned1.sims.nrc.ca.

1090-7807/00 $35.00

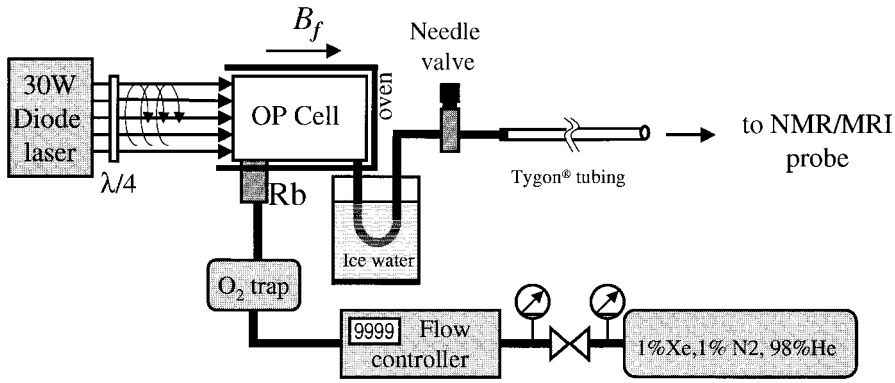

FIG. 1. Diagram of the continuous flow system used for production of optically polarized xenon. The polarization cell and laser are positioned such that the laser beam (circularly polarized) is aligned with the direction of the fringe field of the superconducting magnet.

simple flow system of general utility that produces HP Xe at low partial pressure and high polarization and that can be integrated easily into existing probe technology. Working at low pressure significantly facilitates experimental procedures and thus makes the technique generally accessible. The signal enhancement is sufficiently large that adsorption processes in zeolites and other porous materials can be monitored in real time. Also, by delivering a constant concentration of hyperpolarized xenon to the sample, the acquisition of chemical-shift-resolved images can be achieved in a reasonable length of time. The addition of chemical shift contrast dramatically broadens the scope for HP xenon applications to the studies of a variety of porous materials.

EXPERIMENTAL

Optical polarization of xenon was achieved with an apparatus similar to that described in Ref. (*15*), with the optical pumping cell in the fringe field of the spectrometer magnet. The diagram of the apparatus is shown in Fig. 1. The system is designed to work with a gas mixture consisting of 1% Xe (natural isotope distribution), 1% N_2, 98% He (purchased from Air Products Co.). A standard oxygen purifier (Matheson) reduces oxygen and water impurities in the gas mixture to acceptable levels. As a source of polarizing light we use a 30-W diode laser from Opto-Power Co. After leaving the polarization cell, gas passes through a U-tube placed in an ice bath to remove any entrained Rb. At the needle valve the gas pressure is reduced from 10 bar to slightly above atmospheric and is delivered to the detection region via ~4 m of 3-mm-ID plastic tubing. The flow rate is monitored with an electronic flow meter (Vacuum General, Inc., Model No. US2-31) and is kept constant between 100 and 500 scc/min (scc/min − flow rate normalized to standard conditions − 1 atm and 293 K). At a typical flow rate of 200 scc/min it takes the gas about 9 s to move from the polarizer to a sample and nearly $\frac{1}{3}$ s to pass through the sample region. The polarization level of ^{129}Xe in the mixture is typically in the range from 5 to 6% as checked by comparing the NMR signal intensity with those from sealed standards of xenon–oxygen mixtures. One should note that the pressure reduction to near-atmospheric immediately after the pumping cell significantly facilitates gas delivery to the detection region of the NMR instrument. This approach differs significantly from previous designs (*8–10*), where a closed recirculating system was used at a pressure of 6–10 atm.

CaA and NaY zeolites were commercial samples from Union Carbide. Before use, both were calcined in air at 573 K in order to remove adsorbed water. Porous Vycor tubing (6.8-mm OD, 4.4-mm ID) was purchased from Bioanalytical Systems, Inc., and was calcined in oxygen at 773 K to remove organic impurities. The average pore size for the Vycor was 41 Å as determined by nitrogen porosimetry.

All NMR experiments were carried out on a Bruker DSX-400 spectrometer (magnetic field 9.4 T, ^{129}Xe-resonance frequency 110.7 MHz) equipped with Bruker microimaging accessories. The water-cooled gradient system is capable of producing a maximum gradient of 1 T/m with a gradient rise time of about 100 μs. The probe used a 10-mm birdcage resonator.

RESULTS AND DISCUSSION

The pulse sequence used for the chemical shift imaging experiments is shown in Fig. 2 and consists of a single excitation pulse followed by a free precession delay during which phase-encoding is applied (*16, 17*). In this experiment, two dimensions are spatial, and the third dimension is the chemical shift. Slice selection was achieved by applying a gradient G_z during the frequency-selective excitation pulse, which is, however, still sufficiently broadbanded to excite the full range of the ^{129}Xe chemical shifts. The advantages of the sequence are its simplicity, suitability for short T_2, and, most importantly, a low sensitivity to the effects of flow compared to echo-based techniques. $\pi/2$ excitation pulses have been used in all the experiments to maximize the signal, thus using all of the polarization in the sample region. We found that at room

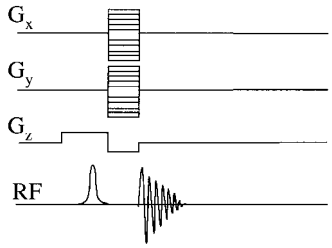

FIG. 2. Pulse sequence used for chemical shift imaging. A frequency-selective 256-μs Hermite pulse with an excitation band of about 16000 Hz was used. G_z is a slice selection gradient and G_x, and G_y are phase encoding gradients. In order to establish a steady-state level of polarization in the sample, between four and eight dummy scans are made before the beginning of acquisition.

temperature and for flow rates above 150 scc/min more than 50% of the xenon polarization was replenished during the recycle delay compared to the original equilibrium polarization without RF pulses. This steady-state polarization remains constant during the entire experiment. One could instead increase the recycle delay in order to replenish the polarization completely, but this would lead to an undesirable increase in the experimental time.

Figure 3 shows a chemical shift image of HP xenon flowing through a phantom consisting of porous Vycor tubing filled with NaY zeolite powder obtained at room temperature. To a certain extent this phantom models a small chemical reactor, as porous Vycor tubes are often used as reactor material for the oxidative coupling of methane (*18*). As well, xenon and methane are very similar in size, and for this reason xenon is often considered a good model for studying adsorption and diffusion properties of CH_4.

Vycor and NaY zeolite have very different pore systems, so that adsorbed xenon has quite distinct chemical shifts in these materials. In the resulting image this is reflected in the separate signals that arise from each region. All three volumes—xenon in the gas phase, in Vycor, and in NaY—have cleanly resolved images. It should be noted that the relaxation times of xenon in both NaY and Vycor are relatively short compared to those reported in previous applications. The ^{129}Xe T_1 is only 1.2 s for NaY and 7 s for Vycor as measured at an equilibrium pressure of 1 atm in thermally polarized gas. It is clear that a short relaxation time is not an obstacle in this instance, and the regions with different porosity can be spatially resolved for macroscopic samples.

Figure 3d shows a 1D spectrum for the sample described above. This spectrum was acquired in a single scan and demonstrates the great sensitivity of the HP ^{129}Xe NMR experiment.

Measurements as a function of xenon loading are an important part of studies of pore space in molecular sieves and other adsorbents. Combining this with CS-resolved imaging, one can identify not only the nature of the pores accessible to xenon, but also where these pores are located. In experiments with adsorption of xenon from the flowing gas, the amount of adsorbed xenon can be controlled by changing either the temperature of the experiment or the partial pressure of the xenon in the flowing mixture. The latter parameter does not need to be changed before the polarizer as it is easy to add some nonpolarized xenon into the stream after the polarization cell. The sensitivity of the experiment does not suffer, as almost the same number of polarized xenon atoms is delivered to the surface in either experiment.

Figure 4 demonstrates a situation where CaA and NaY zeolites are present together. The differences in the structure, size of the voids, and the nature of the charge-compensating cations are reflected in the different chemical shifts of xenon. The spatial resolution of the CS images for the two-zeolite regions is remarkable. It should also be pointed out that it is not necessary to have sharp physical boundaries to differentiate regions of different porosity as in the above example: the experiment will work as long as xenon exchange between different regions remains slow on the NMR time scale. Generally, fast exchange between different regions will result in decreased spatial resolution.

Because CSI requires so many encoding steps it is not possible to execute this experiment using batch mode production of HP xenon. On the other hand, CS imaging is particularly well suited to experiments with flowing HP xenon as it does not involve echo formation, thus circumventing the severe echo attenuation caused by flowing gas in the usual gradient echo techniques. To produce the CS images shown in Figs. 3

FIG. 3. HP ^{129}Xe chemical shift images of a phantom (a) consisting of a 6.8-mm porous Vycor tube packed with NaY zeolite powder ($\sim$250 μm) and placed inside an open 9-mm-ID and 2.5-cm-long glass tube. A 3D image with one spectroscopic and two spatial dimensions is shown (b) together with the sections taken at the indicated chemical shifts (c). Dashed lines indicate the position of the walls of the glass tube. A 1D ^{129}Xe NMR spectrum of the phantom taken in a single scan is shown in (d). The CS image was acquired in a matrix of 40 $\times$ 40 $\times$ 128 points and a square field of view of 20 mm. At the maximum, phase gradients G_x and G_y reached 42 G/cm each. Two scans per each encoding step were made. The flow rate of the gas mixture was 200 scc/min and the total experimental time was 30 min. The 4-mm-thick slice was approximately in the middle of the cylinder. The slice selection gradient G_z was 34 G. During processing, the original matrix was zero-filled to 128 $\times$ 128 $\times$ 256. The 76-ppm chemical shift region corresponds to xenon adsorbed in porous Vycor, the region at 60 ppm to NaY, and that at 0.6 ppm to the interstitial xenon gas.

FIG. 4. HP ^{129}Xe chemical shift image obtained from a 9-mm-ID glass tube filled with pellets of CaA and NaY zeolites, as shown in the top diagram (a). A 3D image with two spatial and one spectroscopic dimensions is shown (b) together with the sections taken at the indicated chemical shifts (c). A 1D ^{129}Xe spectrum is shown at the bottom (d). Experimental conditions were the same as for Fig. 3 except only one scan per encoding step was made. The 93-ppm chemical shift region corresponds to xenon adsorbed in CaA zeolite, the region at 58 ppm to NaY, and that near 0.5 ppm to xenon in the interparticle space.

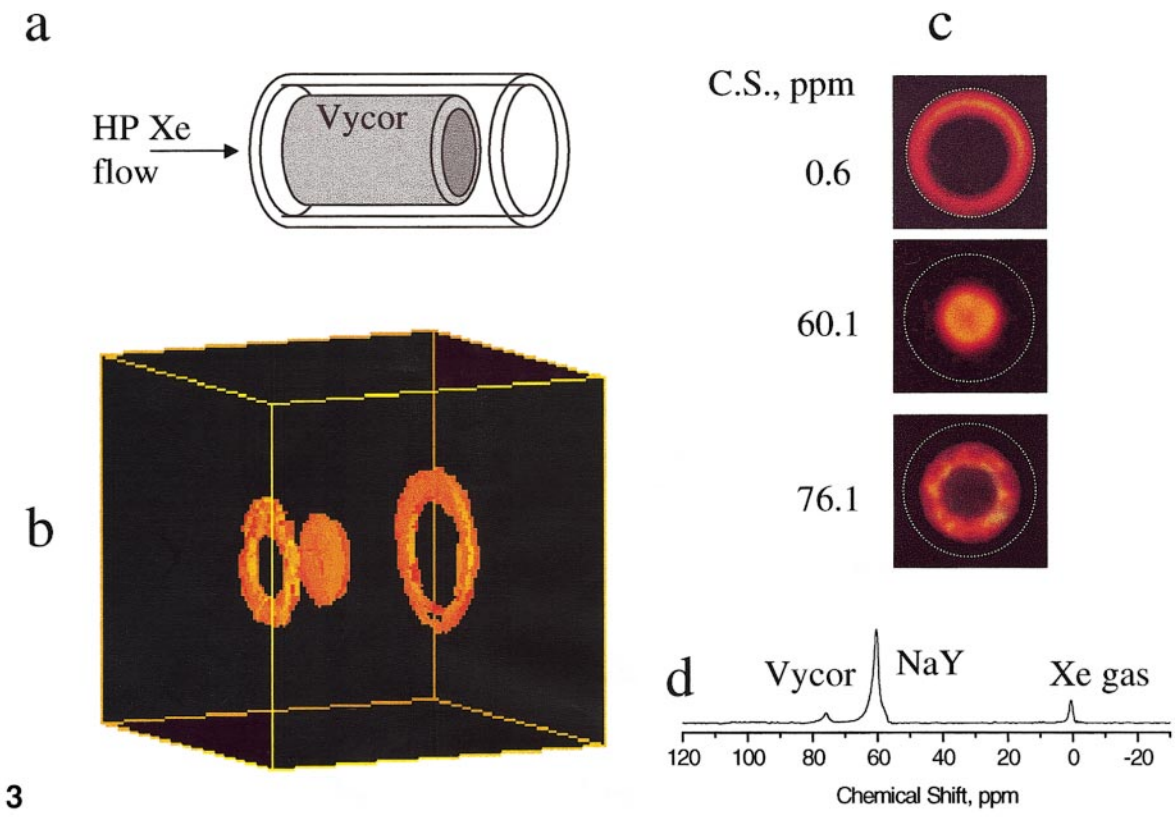
a
HP Xe
flow
Vycor
b
c
C.S., ppm
0.6
60.1
76.1
d
Vycor
NaY
Xe gas
120 100 80 60 40 20 0 -20
Chemical Shift, ppm

3

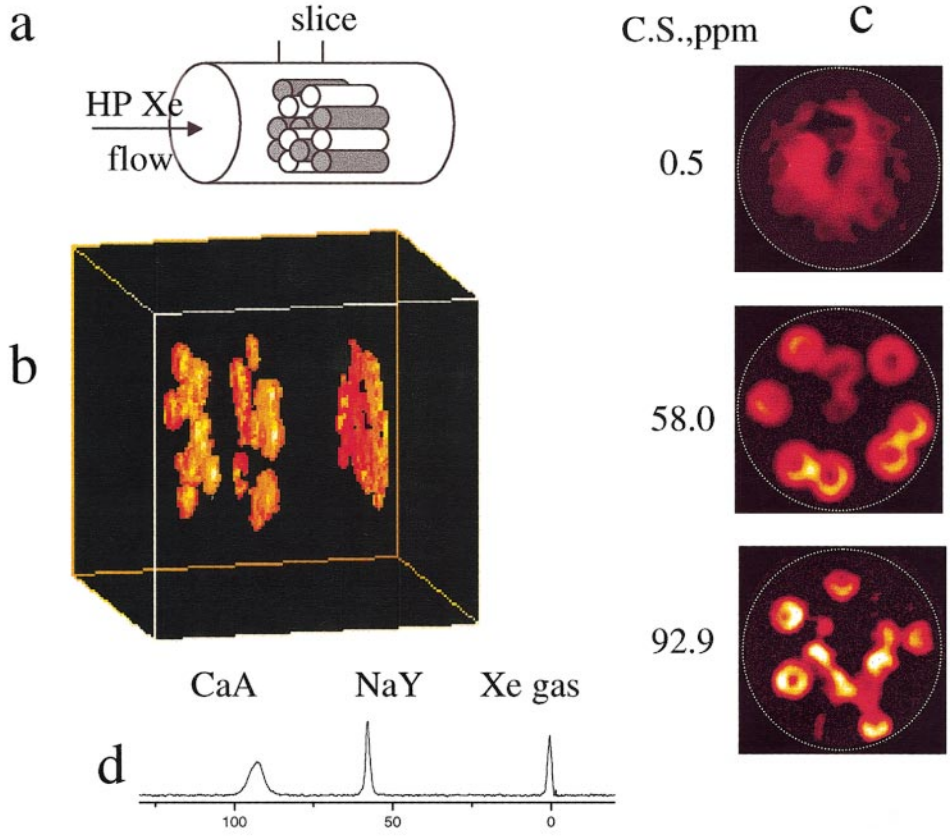
a
slice
HP Xe
flow
b
C.S.,ppm
c
0.5
58.0
92.9
CaA
NaY
Xe gas
d
100
50
0

4

and 4 required only 30 and 15 min, respectively. In fact, the total imaging time could be further reduced if the approaches described in Ref. (*19*) were used. Alternatively, one can increase the resolution of the images at the expense of a longer acquisition time.

A further extension of the experiment would be CS imaging with encoding in all three spatial dimensions, thus requiring the addition of one additional phase encoding gradient and, obviously, the lengthening of the acquisition time. Nevertheless, considering the simplicity of the experimental setup and the fact that not all systems require high spatial resolution, the experiment seems to be generally feasible and useful. Another possible application is the spectroscopy of localized regions. In this case a certain region in 3D space can be selected using frequency-selective pulses in the presence of gradients, and spectroscopic information can be obtained from only the selected region. The simplest combination would be to employ either frequency-selective pulses (*20*) or sandwiches of frequency-selective and -nonselective pulses (*21*) in combination with three orthogonal slice-selective gradients resulting in a cube-shaped volume. With the approaches outlined in Ref. (*21*) this would be essentially a single-scan experiment, and the changes in the selected region induced by adsorption of a second component or some chemical transformations could be followed in real time.

Because it is so easy to work with the open flow system, applications of HP xenon as a tracer become possible for processes such as the thermal modification of void space or adsorption and diffusion of sorbents. Experiments of this kind are underway in our laboratory.

In conclusion, we have reported the first instance of chemical shift imaging of materials with hyperpolarized xenon. We have shown that using HP xenon flow one can produce excellent CS images of various adsorbents in practical, useful times. The method can be applied to materials with relatively short relaxation times and it is expected to be particularly useful in the characterization of complex, multicomponent porous materials. Moreover, the integration of this relatively straightforward continuous flow system into existing probe technology puts such techniques within easy reach of the wider NMR community.

ACKNOWLEDGMENTS

The authors thank M. Vandenhoff, J. Bennett, and J. Farnand for technical assistance and gratefully acknowledge the award of an NRC/NSERC/Industry Partnership grant used in partial support of this work.

REFERENCES

1. T. Ito and J. Fraissard, ^{129}Xe NMR study of xenon adsorbed on Y zeolites, *J. Chem. Phys.* **76,** 5225–5229 (1982).
2. J. A. Ripmeester, Nuclear shielding of trapped xenon obtained by proton-enhanced, magic-angle spinning ^{129}Xe NMR spectroscopy, *J. Am. Chem. Soc.* **104,** 289–290 (1982).
3. (a) C. I. Ratcliffe, Xenon NMR, *Ann. Rep. NMR Spectr.* **36,** 124 (1998); (b) D. Raftery and B. F. Chmelka, Xenon NMR spectroscopy, *NMR Basic Princ. Progr.* **30,** 111–158 (1994); (c) P. J. Barrie and J. Klinowski, ^{129}Xe NMR as a probe for the study of microporous solids: A critical review, *Progr. NMR Spectrosc.* **24,** 91–108 (1992).
4. (a) C. J. Jameson, A. K. Jameson, B. I. Baello, and H.-M. Lim, Grand canonical Monte Carlo simulations of the distribution and chemical shifts of xenon in the cages of zeolite NaA. I. Distribution and ^{129}Xe chemical shifts, *J. Chem. Phys.* **100,** 5965–5976 (1994); (b) C. J. Jameson, A. K. Jameson, H.-M. Lim, and B. I. Baello, Grand canonical Monte Carlo simulations of the distribution and chemical shifts of xenon in the cages of zeolite NaA. II. Structure of adsorbed fluid, *J. Chem. Phys.* **100,** 5977–5987 (1994); (c) C. J. Jameson, A. K. Jameson, and H.-M. Lim, Competitive adsorption of xenon and argon in zeolite NaA. ^{129}Xe nuclear magnetic resonance studies and grand canonical Monte Carlo simulations, *J. Chem. Phys.* **104,** 1709–1728 (1996).
5. (a) B. C. Grover, Noble-gas NMR detection through noble-gas–rubidium hyperfine contact interaction, *Phys. Rev. Lett.* **40,** 391–392 (1978); (b) W. Happer, E. Miron, S. Schaefer, D. Schreiber, W. A. van Wingaarden, and X. Zeng, Polarization of the nuclear spins of noble-gas atoms by spin exchange with optically pumped alkali-metal atoms, *Phys. Rev. A* **29,** 3092–3110 (1984).
6. (a) M. S. Albert, G. D. Cates, B. Driehuys, W. Happer, B. Saam, C. S. Springer, and A. Wishnia, Biological magnetic resonance imaging using laser-polarized ^{129}Xe, *Nature* **370,** 199–201 (1994); (b) J. Mugler III, B. Driehuys, J. Brookeman, G. D. Cates, S. Berr, R. G. Bryant, T. M. Daniel, E. E. de Lange, J. H. Downs III, C. J. Erickson, W. Happer, D. P. Hinton, N. F. Kassel, T. Maier, C. D. Phillips, B. Saam, K. L. Sauer, and M. E. Wagshul, MR imaging and spectroscopy using hyperpolarized ^{129}Xe gas: Preliminary human results, *Magn. Res. Med.* **37,** 809–815 (1997).
7. D. Raftery, E. MacNamara, G. Fisher, C. V. Rice, and J. Smith, Optical pumping and magic angle spinning: Sensitivity and resolution enhancement for surface NMR obtained with laser-polarized xenon, *J. Am. Chem. Soc.* **119,** 8746–8747 (1997).
8. M. Haake, A. Pines, J. A. Reimer, and R. Seydoux, Surface-enhanced NMR using continuous-flow laser-polarized xenon, *J. Am. Chem. Soc.* **119,** 11711–11712 (1997).
9. R. Seydoux, A. Pines, M. Haake, and J. A. Reimer, NMR with continuously circulating flow of laser-polarized ^{129}Xe, *J. Phys. Chem. B* **103,** 4629–4637 (1999).
10. E. Brunner, M. Haake, L. Kaiser, A. Pines, and J. A. Reimer, Gas flow MRI using circulating laser-polarized ^{129}Xe, *J. Magn. Reson.* **138,** 155–159 (1999).
11. Y.-Q. Song, H. C. Gaede, T. Pietrass, G. A. Barrall, G. C. Chingas, M. R. Ayers, and A. Pines, Spin-polarized ^{129}Xe gas imaging of materials, *J. Magn. Reson. A* **115,** 127–130 (1995).
12. (a) X. J. Chen, H. E. Möller, M. S. Chawla, G. P. Cofer, B. Driehuys, L. W. Hedlund, and G. A. Johnson, Spatially resolved measurements of hyperpolarized gas properties in the lung in vivo. Part I: Diffusion coefficient, *Magn. Reson. Med.* **42,** 721–728 (1999); (b) X. J. Chen, H. E. Möller, M. S. Chawla, G. P. Cofer, B. Driehuys, L. W. Hedlund, and G. A. Johnson, Spatially resolved measurements of hyperpolarized gas properties in the lung in vivo. Part II: T_2^*, *Magn. Reson. Med.* **42,** 721–728 (1999).
13. S. D. Swanson, M. S. Rosen, B. W. Agranoff, K. P. Coulter, R. C. Welsh, and T. E. Chupp, Brain MRI with laser-polarized ^{129}Xe, *Magn. Reson. Med.* **38,** 695–698 (1997).
14. D. M. Gregory, R. E. Gerald II, and R. E. Botto, Pore-structure determinations of silica aerogels by ^{129}Xe NMR spectroscopy and imaging, *J. Magn. Reson.* **131,** 327–335 (1998).

15. B. Driehuys, G. D. Cates, E. Miron, K. Sauer, D. K. Walter, and W. Happer, High-volume production of laser-polarized Xe-129, *Appl. Phys. Lett.* **69,** 1668–1670 (1996).

16. P. T. Callaghan, "Principles of Nuclear Magnetic Resonance Microscopy," Clarendon Press, Oxford, 1991.

17. M. Decorps, R. Dupeyre, C. Remy, Y. Le Fur, P. Devoulon, and D. Bourgeois, Spectroscopic imaging, *in* "Magnetic Resonance Spectroscopy in Biology and Medicine: Functional and Pathological Tissue Characterization" (J. D. De Certaines, W. M. M. J. Bovee, and F. Podo, Eds.), Pergamon Press, Oxford, 1992.

18. A. M. Ramachandra, Y. Lu, Y. H. Ma, W. R. Moser, and A. G. Dixon, Oxidative coupling of methane in porous Vycor membrane reactors, *J. Membr. Sci.* **116,** 253–264 (1996).

19. R. E. Gerald II, A. O. Krasavin, and R. E. Botto, A selective-echo method for chemical shift imaging of two-component systems, *J. Magn. Reson. A* **123,** 201–206 (1996).

20. R. J. Ordridge, A. Connelly, and J. A. B. Lohman, Image-selected *in vivo* spectroscopy (ISIS). A new technique for spatially selective NMR spectroscopy, *J. Magn. Res.* **66,** 283–294 (1986).

21. W. P. Aue, S. Müller, T. A. Cross, and J. Seelig, Volume-selective excitation. A novel approach to topical NMR, *J. Magn. Reson.* **56,** 350–354 (1984).